

High Capacity Imaging and Object Identification with Correlated Orbital Angular Momentum Spectroscopy

Casey A. Fitzpatrick,¹ David S. Simon,^{1,2} and Alexander V. Sergienko^{1,3,4}

¹*Dept. of Electrical and Computer Engineering,*

Boston University, 8 Saint Mary's St., Boston, MA 02215

²*Dept. of Physics and Astronomy, Stonehill College, 320 Washington Street, Easton, MA 02357*

³*Photonics Center, Boston University, 8 Saint Mary's St., Boston, MA 02215*

⁴*Dept. of Physics, Boston University, 590 Commonwealth Ave., Boston, MA 02215*

The method of correlated orbital angular momentum (OAM) spectroscopy is shown to be capable of image reconstruction for complex, off-axis objects, with information extraction rates exceeding one bit per photon. Computer simulations of OAM-correlated beams are combined with digitized representations of opaque objects in order to study various effects of the object on the joint OAM coincidence spectrum. It is shown through simulations of OAM-correlated beams that complex image identification and even reconstruction is possible without any measurement in position space. In addition to demonstrating the novel image reconstruction capabilities of this correlation method, the unique off-diagonal spectral signatures, as well as the mutual information rates associated to each object studied, are presented. In particular, changes in these properties due to off-axis translation in the beam field are considered; it is shown that spectral signatures and information rates are independent of environmental factors sufficiently far from the beam center. The results suggest further application in small-scale biological contexts where symmetry and small numbers of noninvasive measurements are important.

I. INTRODUCTION

Recently, a new method of correlated optical sensing was introduced [1], in which correlations between the orbital angular momentum (OAM) states [2–4] of two beams or photons is measured through coincidence counting and singles rates. (See [5–17] for related, *non* OAM-based methods such as ghost imaging and compressive ghost imaging.) Aside from predicting image reconstruction capabilities, the method explored in [1] suggested that objects leave an imprint in the off-diagonal components of the joint OAM coincidence spectrum, where the diagonal represents the well-known conservation of OAM [18]. This aspect of theory was confirmed experimentally in [19]. In these experiments it was observed that the joint OAM spectrum of an object signifies simple rotational symmetries of the object in a predictable way, namely that only the off-diagonal components of the spectrum for which $l_o + l_r = N$ are nonzero when the object transmission profile has an N -fold rotational symmetry, where l_o and l_r represent the OAM content of the object and reference beam, respectively. The theory introduced in [1] also suggests a potential imaging scheme based on correlated OAM states, which we will hereafter refer to as *correlated spiral imaging* (CSI) in reference to *digital spiral imaging* [22–24], an interesting related non-imaging spectroscopic method.

Here, we simulate the performance of CSI using substantially more complicated objects than have been previously considered, paying special attention to the information capacity of the method. By "more complicated" we mean objects with complex geometries, a great deal of angular variation, and at off-center positions in the beam field. We use digitized representations of opaque objects to directly compute the necessary amplitudes in

order to study the effects – on spectral signature, image reconstruction accuracy, and mutual information – of linearly translating objects off-axis with respect to the beam's center.

After reviewing the relevant theoretical concepts and discussing their relation to the CSI measurement apparatus in Sec. II B, we present a number of simulations in Sec. III. We show not only that the method successfully images asymmetric off-axis objects, but that the mutual information contained in the off-diagonal elements of the joint OAM spectrum remains above the one bit per photon limit for objects near the beam center, and grows with the size of the object's symmetry group.

II. BACKGROUND

A. Theory

All beams considered will be decomposed into Laguerre-Gauss (LG) modes $|l, p\rangle$, each mode with OAM $l\hbar$ and p radial nodes where l and p are integers [20, 21]. In cylindrical coordinates (r, z, ϕ) , the position space representation of $|l, p\rangle$ in the object plane is given by [26]

$$\langle r, \phi | l, p \rangle = k_p^{|l|} r^{|l|} e^{-r^2/w_0^2} L_p^{|l|}(2r^2/w_0^2) e^{i\phi l}, \quad (1)$$

where $k_p^{|l|}$ is a normalization constant, $L_n^\alpha(x)$ is the generalized Laguerre polynomial of order n , and w_0 is the beam waist [4].

Before discussing the measurement apparatus, it will be useful to develop a sense of how objects may be represented in terms of their effect on OAM states. By considering this representation now, the role of correlation will become more clear later. We use outer products of OAM

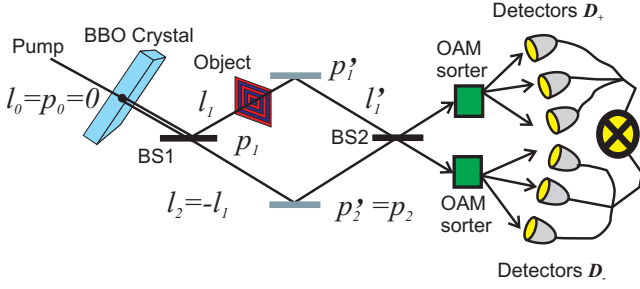


FIG. 1: A setup allowing object image reconstruction via transition amplitude phase-sensitive measurement of correlated OAM content.

states to form an overcomplete basis which can be used to express an object's transmission function, $T(r, \phi)$, as an operator expanded in terms of OAM transitions as follows. For some $a_{p'p}^{l'l} \in \mathbb{C}$

$$\hat{T} = \sum_{l, l', p, p'} a_{p'p}^{l'l} |l', p'\rangle \langle l, p|. \quad (2)$$

To better understand the coefficients $a_{p'p}^{l'l}$, we invert Eq. (2) and find that

$$\begin{aligned} a_{p'p}^{l'l} &= \int dr d\phi [u_{l'p'}(r, \phi)]^* T(r, \phi) u_{lp}(r, \phi) \\ &= \langle l', p' | \hat{T} | l, p \rangle. \end{aligned} \quad (3)$$

Eq. (3) shows that the $a_{p'p}^{l'l}$ are in fact *amplitudes* for a given state $|l, p\rangle$ to transition to the state $|l', p'\rangle$. Since the LG state vectors are *a priori* known basis elements, successful reconstruction of an image depends only on the determination of the $a_{p'p}^{l'l}$, as indicated by Eq. (2). We note here a clear analogy with Fourier decomposition, with the exception that our basis functions form an overcomplete basis.

B. Apparatus

We will now explain how the transition amplitudes, $a_{p'p}^{l'l}$ of Eq. (3), may be recovered using the correlation setup shown in Fig. 1. As a source of photon pairs which are correlated in OAM, consider a Gaussian pump, $|l_p, p_0\rangle = |0, p_0\rangle$, producing object and reference beams, $|l_1, p_1\rangle$ and $|l_2, p_2\rangle$ respectively, via (collinear) spontaneous parametric down-conversion (SPDC); type I or type II SPDC will suffice, however coincidence coincidence rates are higher for type II SPDC with a polarizing beam splitter [1, 24–28]. The beams, anti-correlated in OAM since $l_p = l_1 + l_2$, are then directed into separate branches by a 50:50 beam-splitter (see Fig. 1). The presence of the object will cause the state of a photon in the

object beam to transition from $|l_1, p_1\rangle$ to $|l'_1, p'_1\rangle$, while the state of the reference photon remains unchanged. The object's OAM transition amplitude is precisely what we seek to recover.

By inserting an additional beam splitter before sorting the states, amplitude path-mixing is induced (see Fig. 1). The resulting detection *amplitudes* in the upper (D_+) and lower (D_-) detectors are, respectively, proportional to $|a_{p_1 p_1}^{l'_1 l_1} + i|$ and $|ia_{p_1 p_1}^{l'_1 l_1} + 1|$, neglecting overall constants (Note that the amplitudes associated to $|l_2, p_2\rangle$ are 1 since no transition takes place, hence those quantum numbers do not appear in the beam splitter expressions.) The proportionality constant is determined by the weighting coefficients associated to the SPDC process [26]. This means that the singles count rates N_+ and N_- in each detector are given by

$$N_+ \approx |a_{p_1 p_1}^{l'_1 l_1} + i|^2 \quad (4)$$

$$N_- \approx |ia_{p_1 p_1}^{l'_1 l_1} + 1|^2. \quad (5)$$

We assume perfect detectors; imperfections can be accounted for by methods described in [26]. The singles rate equations can now be used to express both the real and imaginary parts of the $a_{p_1 p_1}^{l'_1 l_1}$. However, we must only use singles rates associated to coincidence events. Thus, using the real part, $\Re(a_{p_1 p_1}^{l'_1 l_1}) = \sqrt{N_+ - 1 - \frac{1}{16}(N_+^2 - N_-^2 - 2N_+ N_-) - \frac{1}{2}(N_+ - N_-)}$, and the imaginary part, $\Im(a_{p_1 p_1}^{l'_1 l_1}) = \frac{1}{4}(N_+ - N_-)$ of $a_{p_1 p_1}^{l'_1 l_1}$, alongside coincidences, we now have all necessary information for image reconstruction.

Finally, let $P(l_1, p_1; l_2, p_2)$ be the mutual probability for detecting signal with quantum numbers l_1, p_1 and idler with values l_2, p_2 . The marginal probabilities at the two detectors (probabilities for detection of a single photon, rather than for coincidence detection) are

$$P_s(l_1, p_1) = \sum_{l_2, p_2} P(l_1, p_1; l_2, p_2) \quad (6)$$

$$P_i(l_2, p_2) = \sum_{l_1, p_1} P(l_1, p_1; l_2, p_2). \quad (7)$$

Then the mutual information for the pair is

$$\begin{aligned} I(s, i) &= \sum_{l_1, l_2 = l_{min}}^{l_{max}} \sum_{p_1, p_2 = 0}^{p_{max}} P(l_1, p_1; l_2, p_2) \\ &\times \log_2 \left(\frac{P(l_1, p_1; l_2, p_2)}{P_s(l_1, p_1) P_i(l_2, p_2)} \right) \end{aligned} \quad (8)$$

The setup in Fig. 1 can be used, accounting for the SPDC weighting coefficients, to generate OAM coincidence spectra, as we shall see in Sec. III. Alternatively,

one can simply remove the second beam splitter and measure the coincidences directly; images will not be attainable since only the transition amplitude magnitudes will be known, but the spectral signature of objects may still be obtained [1, 19]. Which version of the setup one uses will depend on the application at hand, in particular whether or not an image is desired or a spectral signature will suffice.

So far we have assumed the experimenter has the ability to discriminate different p values while sorting OAM states. However, in reality such a discrimination is beyond current experimental means [28]. Therefore, to demonstrate the full implications of the above detection method, we must (presently) rely on simulation methods, described in Sec. III.

III. IMAGING AND INFORMATION

Successful imaging of any object that has significant radial structure with CSI requires the ability to discriminate OAM states with $p > 0$, since the expansion basis for \hat{T} depends upon distinct contributions from each (p', p) combination in the set of basis states (see Eq. (2)). In the simulations below, we use digitized representations of various opaque objects to directly compute Eq. (3) in order to study the effects – on spectral signature, image reconstruction accuracy, and mutual information – of translating the target objects off-axis with respect to the beam’s center. In addition to image reconstructions we show many joint OAM coincidence spectra and use these spectra to perform mutual information calculations using Eq. (8). As discussed Sec. IIB, the spectra may be constructed from singles measurements combined with coincidence measurements and the addition of a second beam splitter before detection (as we simulate here), or, directly measured in a coincidence-only setup, with no second beam splitter, as in [19]. Although the nature of the simulations requires some stored information about the objects (namely, their transmission profiles are stored as matrices of zeros and ones), we would like to stress that the measurement apparatus requires *no* optical components to be placed in the vicinity of objects. Thus the following simulations outline a remote OAM-based imaging and object recognition technique that can be tested experimentally as soon as reliable methods for distinguishing $p > 0$ states are developed.

A. Imaging Complex Objects

The experimental results of [19] briefly discuss the role of symmetry in an object’s joint OAM spectrum. The most important point for our purposes is that objects with simple N -fold rotational symmetry leave their imprint on the *off-diagonal* (in particular, the $l_o + l_r = N$) elements of the joint spectrum. More generally, suppose that the object has a rotational symmetry group of order

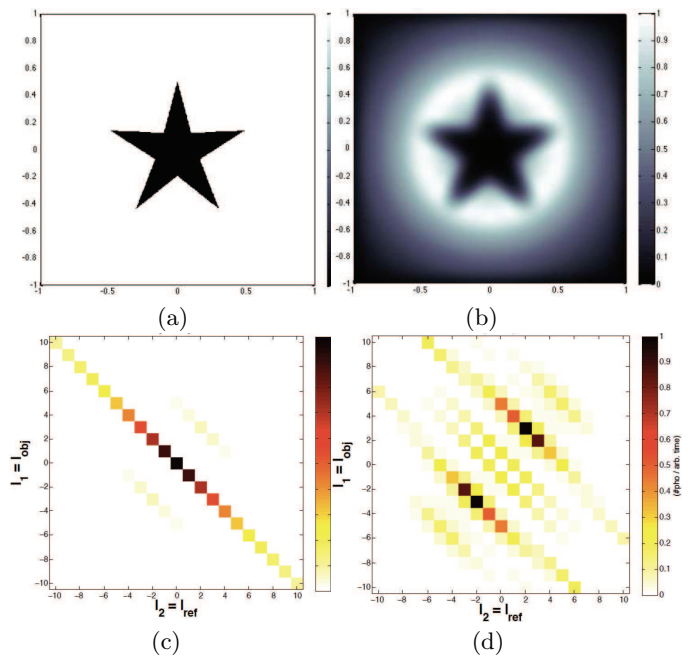


FIG. 2: (a) Opaque star object of max width $0.9w_0$ and, (b) the CSI reconstruction using $l_{max} = 10$, $p_{max} = 7$; (c) The joint OAM spectrum of the star, having summed over all p , and (d) the same spectrum with the conservation diagonal removed.

N ; i.e., it is invariant under $\phi \rightarrow \phi + \frac{2\pi}{N}$. From Eqs. (2) and (3) it follows that the coefficients must then satisfy $a_{p'_1 l'_1}^{l_1} = e^{\frac{2\pi i}{N}(l'_1 - l_1)} a_{p'_1 l'_1}^{l_1}$, which implies $a_{p'_1 l'_1}^{l_1} = 0$ except when $\frac{l'_1 - l_1}{N}$ is integer. When N goes up (enlarged symmetry group), the number of nonzero $a_{p'_1 l'_1}^{l_1}$ goes down; with the probability concentrated in a smaller number of configurations, correlations increase and mutual information goes up, as we will see below.

It is also worth noting that the objects used in [19], while having width much smaller than the beam waist, had length that extended far beyond the beam radius.

Fig. 2(b) shows the joint spectrum of a simple 5-pointed opaque star (with 5-fold rotational symmetry) whose dimensions are confined entirely within the beam. The object’s lack of radial extension causes a decrease in magnitude of the $l = \pm 5$ components of the joint spectrum, since the LG modes of higher momentum (higher l) do not interact with the object. Consequently, the object’s spectral signature in the off-diagonal components of the joint OAM spectrum becomes visually less obvious. However, as Fig. 2(d) shows, by setting the diagonal components of the joint spectrum to 0 and rescaling the colormap used to view the spectrum, the off-diagonal contributions become much more visible. Since it is these off-diagonal contributions that carry the extra information upon which the CSI setup is based, in order to improve the contrast of off-diagonal spectral components, we will zero out the conservation diagonal (states with

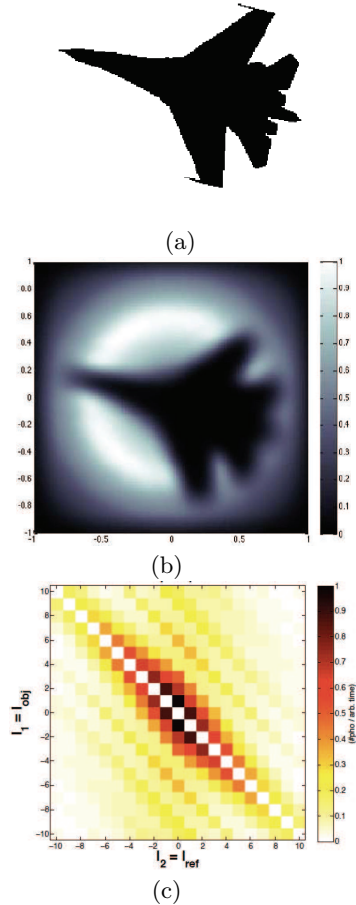


FIG. 3: (a) Opaque fighter jet object of max width w_0 and, (b) the CSI reconstruction using $l_{max} = 10$, $p_{max} = 7$; (c) The joint OAM spectrum of the fighter jet, summed over all p with the conservation diagonal removed.

($l_o = -l_r$) for the remaining object spectra simulated in this report. The image reconstructions will include the contributions of the $l_o = -l_r$ states.

Figs. 3(b) and 4(b) simulate the ability of the CSI method to image objects with more complicated, less symmetric transmission functions $T(r, \phi)$. The joint spectra shown in Figs. 4(c) and 3(c) are clearly less compact than those of simpler objects, like the star. This is to be expected when one views complicated objects as a superposition of many simpler, symmetric objects translated with respect to the beam axis: as shown below (Sec. IIIB), translation with respect to the beam axis, even for simple objects, spreads the joint spectrum.

B. Off-Axis Translation and Mutual Information

In Figs. 5, 6, and 7 we show the image reconstruction and spectral signatures of the same objects shown in Figs. 2, 3, and 4 respectively *after having been shrunk*

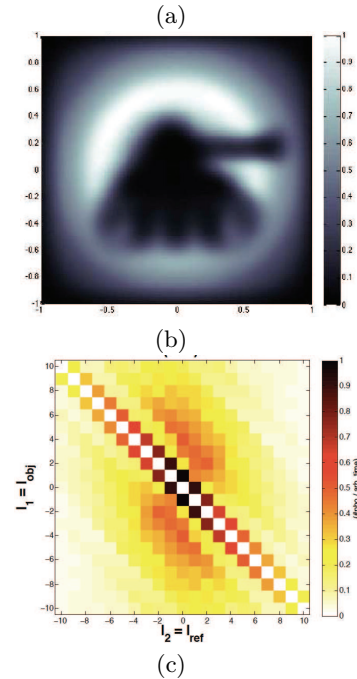


FIG. 4: (a) Opaque tank object of max width $0.7w_0$ and, (b) the CSI reconstruction using $l_{max} = 10$, $p_{max} = 7$; (c) The joint OAM spectrum of the tank, summed over all p with the conservation diagonal removed.

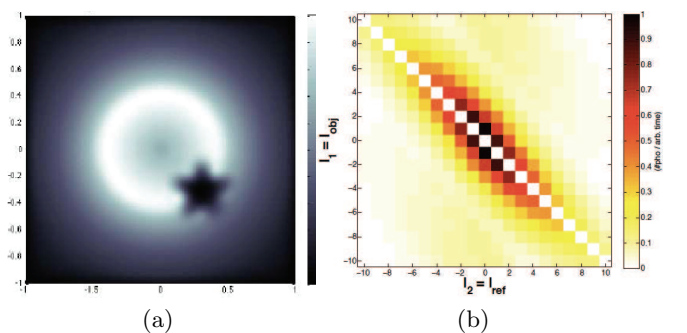


FIG. 5: (a) The CSI reconstruction of a translated opaque star, using $l_{max} = 10$, $p_{max} = 7$; (b) The joint OAM spectrum of the translated star, summed over all p with the conservation diagonal removed.

by a factor of 4 and translated radially with respect to the beam axis by approximately $0.7w_0 - 0.9w_0$. The effect of translation is most obvious in the case of the star, whose centered spectral signature is quite sparse compared to

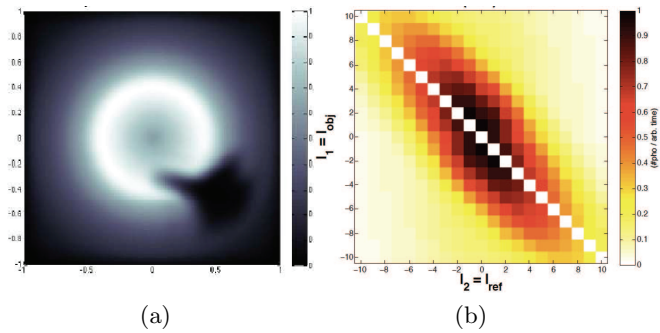


FIG. 6: (a) The CSI reconstruction of a translated opaque fighter jet, using $l_{max} = 10$, $p_{max} = 7$; (b) The joint OAM spectrum of the fighter jet, summed over all p with the conservation diagonal removed.

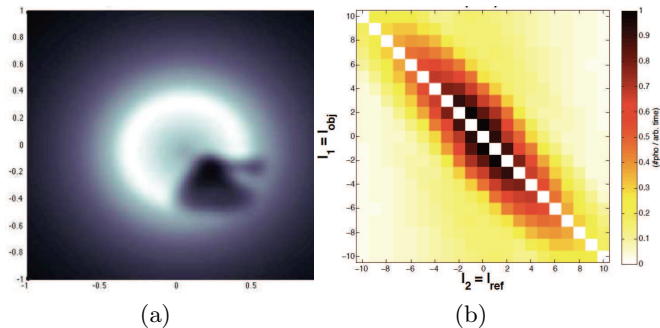


FIG. 7: (a) The CSI reconstruction of a translated opaque tank, using $l_{max} = 10$, $p_{max} = 7$; (b) The joint OAM spectrum of the tank, summed over all p with the conservation diagonal removed.

those of the tank or fighter jet. Namely, we observe that translation with respect to the beam axis causes a *spreading* in the spectral distribution. Although the exact dynamics of the spectral spread caused by translation vary from object to object, we note that once the object is sufficiently far from the beam center – not surprisingly – the conservation diagonal is all that remains, all off-diagonal components going to zero.

Given the variation in spectral signature as the object is translated through the beam field, we expect to see a corresponding variation in the mutual information carried by the components of the joint OAM spectrum. To calculate this change, we simulated the spectra of the above objects several times, linearly translating them with each iteration, starting from the beam center and ending effectively outside of the beam field completely. For each position the mutual information was calculated using Eq. (8), and the results are plotted as a function of distance in Fig. 8. Since we are in this study primarily interested in the information content of the heretofore unconsidered off-diagonal components of the joint OAM spectrum, we again zero out the conservation diagonal for all spectra so that *the mutual information calculated represents information carried exclusively by off-diagonal components of the spectrum*.

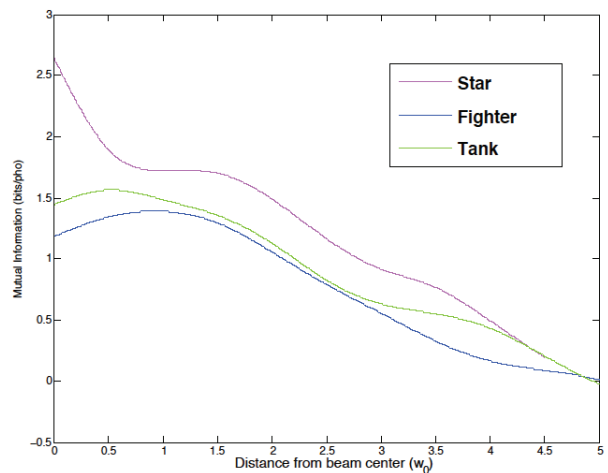


FIG. 8: Mutual information carried by off-diagonal components of joint OAM spectrum, for various objects, as a function of distance from beam center with $l_{max} = 10$, $p_{max} = 5$; increasing p_{max} will increase the mutual information substantially. Note that each object's off-diagonal information content exceeds one bit per photon at the beam center.

We see that *even for complex objects near the beam center, the mutual information carried by off-diagonal components of the joint OAM spectrum exceeds one bit per photon*. As expected, the information goes to zero as the object moves sufficiently far from the beam center. Note that the simpler the object here – the star – carries the most off-diagonal information, consistent with the argument made in Sec. III A, that enlarged symmetry groups cause an increase in correlations which in turn causes the mutual information to go up. In fact, as we increase p_{max} and the objects' symmetries are better approximated, the mutual information for each object goes up. In Fig. 8, $p \in (0, 3)$ with the star's $I_{max} \approx 2.6$ bits/pho. Increasing p_{max} to 7 gives an $I_{max} \approx 3.3$ bits/pho in off-diagonal components.

C. Discussion

The above simulations demonstrate the informational capacity of off-diagonal components in the joint OAM spectra. We have exploited this capacity for the purposes of imaging and object identification by way of the joint OAM spectral signature. Current experimental barriers, namely the inability to easily detect $p > 0$ modes at the single photon level, present difficulties in physically implementing the experimental apparatus required to recover the phases of the amplitudes needed for image reconstruction. However, as our simulations indicate, such an apparatus would be capable of using the information contained in the off-diagonal components of the joint OAM spectrum to remote image unknown objects *without any record of the spatial distribution of the photons measured*.

IV. CONCLUSIONS

The spectral signatures simulated in the final sections of this letter rely only on coincidence measurements. This means that, where a set of objects with unique signatures or symmetries is in question, our method can be used to detect the presence or absence of objects in question in relatively few measurements as compared to pixel-by-pixel imaging methods.

A number of novel applications suggest themselves based on the results above. For example, note that if the object is rotated, the outgoing OAM states simply pick up an overall phase that does not affect the joint OAM spectrum. This could be useful, because it allows a rapidly rotating object to be identified from its OAM spectrum using slow detectors and a small number of measurements. In some circumstances, this may be less expensive and more practical than the use of high speed cameras.

The high mutual information capacity of off-diagonal OAM spectral components also makes our method well suited for sensing rotational symmetries in few measurements. Due to the fragility of OAM states, the advantages of our setup may best be exploited in small scale biological or production contexts. For example, the scanning of a biological sample using correlated OAM measurements may enable efficient detection of the presence or absence of certain structures based on the comparison of theoretical and observed coincidence rates of off-

diagonal spectral components. And, since objects sufficiently far from the beam center do not affect the coincidence rates, as seen by the mutual information plots in Fig. 8, we can be confident that a sufficiently small beam waist will yield accurate spectra. Biological *apoptosis* (so-called programmed cell death) is one context in which the presence or absence of cell symmetries plays an important role, since apoptotic cells lose their symmetry, and so a change in the distribution of symmetries may indicate a cancerous sample. Sickle cell anemia may provide another avenue for future research, since normal red blood cells have circular symmetry, but sickle cells do not.

The research above furthers the informational analysis of off-diagonal joint OAM spectral components, in addition to demonstrating the full reach of CSI's imaging capabilities. We have seen that not only do these off-diagonal components carry information that allows image reconstruction, but they do so at rates which can well exceed the bit per photon limit at significant distances from the beam center.

Acknowledgments

This research was supported by the DARPA In-Pho program through US Army Research Office award W911NF-10-1-0404.

-
- [1] D. S. Simon, A. V. Sergienko, *Phys. Rev. A*, **85**, 043825, 2012.
- [2] L. Allen, M. W. Beijersbergen, R. J. C. Spreeuw, and J. P. Woerdman, *Phys. Rev. A* **45**, 8185 (1992).
- [3] S. Franke-Arnold, L. Allen, M. Padgett, *Laser & Photon. Rev.* **2**, 299 (2008).
- [4] A. M. Yao and M. J. Padgett, *Adv. in Opt. & Phot.* **3**, 161(2011).
- [5] D.V. Strekalov, A. V. Sergienko, D. N. Klyshko, and Y. H. Shih, *Phys. Rev. Lett.* **74**, 3600 (1995).
- [6] D. N. Klyshko, *Sov. Phys. JETP* **76**, 1131 (1988).
- [7] A. V. Belinskii and D. N. Klyshko, *Sov. Phys. JETP* **78**, 259 (1994).
- [8] T. B. Pittman, Y. H. Shih, D. V. Strekalov, and A. V. Sergienko, *Phys. Rev. A* **52**, R3429 (1995).
- [9] R. S. Bennink, S. J. Bentley, R. W. Boyd, *Phys. Rev. Lett.* **89**, 113601 (2002).
- [10] R. S. Bennink, S. J. Bentley, R. W. Boyd, J. C. Howell, *Phys. Rev. Lett.* **92**, 033601 (2004).
- [11] O. Katz, Y. Bromberg, and Y. Silberberg, *Appl. Phys. Lett.* **95**, 113110 (2009).
- [12] V. Katkovnik, J. Astola, *J. Opt. Soc. Am. A*, **8**, 1556 (2012).
- [13] B. Jack, J. Leach, J. Romero, S. Franke-Arnold, M. Ritsch-Marte, S. M. Barnett, and M. J. Padgett, *Phys. Rev. Lett.* **103**, 083602 (2009).
- [14] F. Ferri, D. Magatti, A. Gatti, M. Bache, E. Brambilla, L. A. Lugiato, *Phys. Rev. Lett.* **94**, 183602 (2005)
- [15] W. Gong, S. Han, *J. Opt. Soc. Am. A*, **29**, 1571 (2012).
- [16] A. Gatti, E. Brambilla, M. Bache, L. A. Lugiato, *Phys. Rev. Lett.* **93**, 093602 (2004).
- [17] A. Valencia, G. Scarcelli, M. D'Angelo, Y.H. Shih, *Phys. Rev. Lett.* **94**, 063601 (2005).
- [18] A. Mair, A. Vaziri, G. Weihs, A. Zeilinger, *Nature* **412**, 313(2001).
- [19] N. Uribe-Patarroyo, A. Fraine, D. S. Simon, O. Minaeva, A. V. Sergienko, *Phys. Rev. Lett.* **110**, 043601 (2013).
- [20] L. Allen, M. Padgett, M. Babiker, *Prog. Opt.* **39**, 291 (1999).
- [21] M. J. Padgett, L. and Allen, *Opt. Comm.*, **121** 36 (1995).
- [22] G. Molina-Terriza, L. Rebane, J. P. Torres, L. Torner, S. Carrasco, *J. Eur. Opt. Soc.* **2**, 07014 (2007).
- [23] L. Torner, J. P. Torres, S. Carrasco, *Opt. Exp.* **13**, 873 (2005).
- [24] J. P. Torres, A. Alexandrescu, L. Torner, *Phys. Rev. A* **68**, 050301(R) (2003).
- [25] B. E. A. Saleh, A. F. Abouraddy, A. V. Sergienko, and M. C. Teich, *Phys. Rev. A* **62**, 043816 (2000).
- [26] X. F. Ren, G. P. Guo, B. Yu, J. Li and G. C. Guo, *J. Opt. B: Quantum Semiclass. Opt.* **6**, 243 (2004).
- [27] J. Leach, B. Jack, Barry, J. Romero, A. K. Jha, K. Anand, A. M. Yao, S. Franke-Arnold, D. G. Ireland, R. W. Boyd, S. M. Barnett, M. J. Padgett, *Science*, **329**, 662 (2010).

- [28] H. Di Lorenzo Pires, H. C. B. Florijn, M. P. van Exter,
Phys. Rev. Lett., **104**, 020505 (2010).